Transport Policy 83 (2019) 102–110

Contents lists available at ScienceDirect

Transport Policy

journal homepage: www.elsevier.com/locate/tranpol

Potential to reduce the climate impact of aviation by climate restricted airspaces

M. Niklaß[a,*], B. Lührs[b], V. Grewe[c,d], K. Dahlmann[c], T. Luchkova[e], F. Linke[a], V. Gollnick[a,b]

[a] Deutsches Zentrum für Luft- und Raumfahrt (DLR), Lufttransportsysteme, Hamburg, Germany
[b] Technische Universität Hamburg (TUHH), Institut für Lufttransportsysteme, Hamburg, Germany
[c] Deutsches Zentrum für Luft- und Raumfahrt (DLR), Institut für Physik der Atmosphäre, Oberpfaffenhofen, Germany
[d] Delft University of Technology, Aerospace Engineering, Section Aircraft Noise & Climate Effects, Delft, Netherlands
[e] Deutsches Zentrum für Luft- und Raumfahrt (DLR), Institut für Flugführung, Brunswick, Germany

ARTICLE INFO

Keywords:
Operations research
Systems design
Climate mitigation strategy
Air traffic regulation
Cost-benefit analysis
Trajectory optimization
Optimal control

ABSTRACT

Impacts of commercial aircraft operation upon the environment, which are caused primarily from emissions of CO_2, NO_x and the formation of contrails, are matter of growing concern, as aviation is one of the fastest developing industrial sectors worldwide and the awareness of its effects is expanding. Recent research has focused on the cost-benefit potential of different mitigation strategies, which optimize flight trajectories with respect to climate and economy, but most of these mitigation strategies cannot be implemented in the near future due to technical challenges.

The objective of this paper is to present an interim mitigation strategy, which bridges this time period. In analogy to military exclusion zones, climate restricted airspaces (CRA) are defined based on 3-D climate change functions, characterizing the environmental impact caused by an aircraft emission at a certain location. Regions with climate costs greater than a threshold value are closed in the corresponding month; others are cleared for air traffic. To estimate the cost-benefit potential of this strategy, a preliminary analysis is conducted on the route from Helsinki (EFHK) to Miami (KMIA). Affected flight trajectories are re-routed optimally around resulting CRA with regard to monetary costs for varying threshold values. Therefore, flight simulation algorithms are developed, which solve a non-linear optimal control problem. For each optimized flight trajectory corresponding average temperature response (ATR) and cash operating costs (COC) are expressed relative to a reference great circle trajectory with constant Mach number and compared with the climate mitigation potential of climate optimized trajectories.

1. Introduction

Air traffic operations affect climate through the emission of carbon dioxides (CO_2), water vapor (H_2O), aerosols, and nitrogen oxides (NO_x). The latter influences the formation of ozone (O_3) and the depletion of methane (CH_4), both being important greenhouse gases. Emissions of H_2O and aerosols trigger the formation of contrails. The largest amount of these aircraft emissions is emitted during the cruise phase at altitudes, which are particularly sensitive to climate.

In the year 2005 air traffic caused 3.5% of the global anthropogenic radiative forcing (RF), excluding the impact of contrail induced cirrus cloudiness (CiC). Almost two-thirds of aviations RF is triggered by non-CO_2 emissions (Lee et al., 2010). With a predicted annual growth rate of 4.7% (Airbus, 2013), which largely outpaces the estimated annual fuel efficiency improvement rate of 1–2% (Solomon et al., 2007), the environmental effect of aviation will continue to grow.

To reduce the impact of air traffic emissions on global warming, different technological, operational as well as regulative approaches are conceivable. As non-CO_2 emissions are highly dependent on chemical and meteorological background conditions, and characterized by life-times much shorter than that of CO_2, their climate impact largely depends on emission location (altitude, latitude, longitude) and time (time of the day and season). Taking these dependencies into account, the most promising mitigation strategies are optimized flight trajectories, minimizing time and emissions in climate sensitive regions. Several infrastructural constraints, such as air traffic service (ATS) routes and airspace boundaries defined within airspace management (ASM) processes impact the design of operational flight plan trajectories. Air traffic control (ATC) restrictions, such as separation procedures in high-density airspaces may additionally cause the need to adapt planned trajectories. Those restrictions are potentially based on short-term weather predictions. Therefore, due to limited flexibility

* Corresponding author.

http://dx.doi.org/10.1016/j.tranpol.2016.12.010
Received 6 July 2016; Received in revised form 10 November 2016; Accepted 31 December 2016
Available online 08 February 2017

in trajectory design, climate sensitive regions cannot be avoided sufficiently at present. If it is not feasible to predict exactly the position of climate sensitive regions, it is possible that flights would accidentally pass them or would change their flight altitude without need, hence resulting in a lower or negative environmental net benefit. Therefore, the implementation of weather-optimized trajectories requires higher accuracy of wind, temperature and weather prediction, and increased flexibility of ASM- and ATC-related trajectory design (SESAR, 2012; Mulkerin, 2003).

Taking into account the technical challenges mentioned above, most of these mitigation strategies cannot be implemented in the near future. In order to bridge this period, mitigation strategies are necessary, which pursue the same objectives and are easily implementable in the next few years.

A proposal for an interim mitigation strategy is described in Section 2. Section 3 briefly introduces the models used for a first assessment of this strategy. Climate change functions are calculated and climate restricted airspaces defined in Section 4. In Section 5 optimal control techniques are applied. They are used to detour trajectories optimally with regard to COC around the resulting CRA, as well as to calculate trajectories which are optimal with regard to climate and COC (benchmark). A cost-benefit analysis of the first results is presented in Section 6. Since our calculations are still in progress, only preliminary results are shown here.

2. Climate restricted airspaces

In this approach, highly climate sensitive regions are closed for a period of time (e.g. for several hours, a day, or a month) and affected flights are re-routed around them; contrary to approaches of climate optimized trajectories minimizing time and emissions in these regions. Therefore, we introduce climate restricted airspaces, in analogy to military exclusion zones.

The climate change contribution caused by a single flight is measured by total climate change functions (CCF_{tot}) depending on locus and time of CO_2 and non-CO_2 emissions. On the basis of scientific evidence a threshold value for CCF_{tot} is selected by policy makers, which defines the boundary condition between restricted and cleared airspace. Regions with climate costs greater than the threshold value are closed in the corresponding restriction period; others are cleared for air traffic. If a threshold is determined and agreed, CRA can be easily implemented by air traffic control. Thus, global warming of aviation will be mitigated without implementation of complex climate cost algorithms into the flight planning software of the airlines.

The restriction period of an airspace – hours or weeks? – as well as its timing – how far can a CRA be scheduled in advance? – are highly depending on climate agents i taken into consideration and the data-set of CCF – CCF can either be based on climatological mean data ($CCF_{c,i}$) or actual weather forecasts ($CCF_{w,i}$). As CCF_i are calculated individually for each agent i before superposing, these decisions can be adapted any time to current level of scientific understanding (LOSU). For instance, if the CRA concept focuses on avoiding CiC only, three days before departure seems to be a feasible time for the scheduling of CRA, as specialist services, like the European Centre for Medium-Range Weather Forecasts (ECMWF), have a high skill in predicting cold ice-supersaturated regions (Rädel and Shine, 2010). If CCFs are based on actual weather forecasts, restriction periods of few hours are possible. However, the calculation of CCF_w, require daily simulations with comprehensive climate-chemistry models, which are very expensive in terms of time and computational resources, and, therefore, require much more research before they might become operationally available. Until this date, CRA can be based, as a first step, on CCF_c, knowing that much better climate change functions are desirable (e.g. Grewe et al., 2014). CCF_c only have to be calculated once, but do not allow a shorter time resolution than a month. Nevertheless, they are well suited to test the concept of CRAs.

3. Models for environmental and ecological analysis

3.1. Modeling the climate impact with AirClim

Within this study, CCFs are computed by *AirClim*, a model which linearizes the complex functional chain from emissions to climate change, including transport, chemistry, micro-physics, and radiation under consideration of climatological mean data. As climate-chemistry calculations are very expensive in time and computational resources, *AirClim* combines aircraft emission data with pre-calculated altitude and latitude dependent atmospheric data to minimize the calculation time (Grewe and Stenke, 2008; Dahlmann et al., 2016).

The atmospheric data represents the atmospheric sensitivity to regional emissions. They are derived from steady-state simulations with the climate-chemistry model E39/C based on background emissions. Soil and sea surface temperatures as well as background emissions resulting from industry, biomass burning and ground transport are taken from IPCC scenario A1B (Houghton et al., 2001). Aircraft background emissions follow the QUANTIFY emission inventory (Borken-Kleefeld et al., 2010), which temporal evolution is scaled by the IPCC scenario Fa1 (Henderson et al., 1999).

Considering the climate agents CO_2, H_2O, CH_4, O_3, PMO (latter three resulting from NO_x emissions), and CiC, *AirClim* calculates the temporal evolution of atmospheric concentration changes, radiative forcing and near surface temperature changes (hereafter referred as climate costs) as function of latitude and altitude (2-D) for each climate agent, except CiC for which 3-D climate change functions are calculated depending on latitude, longitude and altitude (Grewe and Stenke, 2008; Dahlmann et al., 2016).

3.2. Modeling 4-D emission inventories with the trajectory calculation module

The Trajectory Calculation Module (*TCM*) is applied in order to calculate detailed 4-D trajectories including the corresponding emission inventories. For this purpose, *TCM* performs a time-discrete forward-integration of all relevant aircraft state variables (Lührs et al., 2014; Linke, 2016).

Acceleration and vertical speed of aircraft are regulated to match desired target speeds and altitudes by proportional-integral altitude and speed controllers. Furthermore, aerodynamic drag is obtained using Eurocontrol's Base of Aircraft Data Revision 4.0 (BADA) aircraft performance models (Nuic and Mouillet, 2012). By applying the Total-Energy-Model, the required thrust is calculated serving as input for the BADA 4.0 engine performance models which are used in order to determine the fuel flow. For the CO_2- and H_2O-flows a stoichiometric combustion is assumed; the emission index of NO_x (EI_{NO_x}) is determined based on the Eurocontrol modified Boeing Fuel Flow Method 2 (DuBois and Paynter, 2006; Jelinek et al., 2004).

3.3. Modeling optimized trajectories with the trajectory optimization module

The calculation of optimized 4-D trajectories and their emission inventories is performed by the Trajectory Optimization Module (*TOM*) which is based on an optimal control approach. Hence, a vector of state variables x(t) and control variables u(t) is used to describe the motion of aircraft. Optimal trajectories are obtained by identifying a control input u(t), which minimizes a cost functional $\mathcal{J}$ (see Eq. (1)) while satisfying dynamic constraints (see Eq. (2)) as well as control and state limitations (see Eqs. (3)–(6)).

$$\mathcal{J}(t, \mathbf{x}(t), \mathbf{u}(t)) = c_\Upsilon \cdot \Upsilon(t_0, t_f, \mathbf{x}(t_0), \mathbf{x}(t_f)) + c_\Psi \cdot \int_{t_0}^{t_f} \Psi(\mathbf{x}(t), \mathbf{u}(t), t)\mathrm{d}t \quad (1)$$

$$\dot{\mathbf{x}}(t) = f(\mathbf{x}(t), \mathbf{u}(t), t) \tag{2}$$

$$\mathbf{x}(t_0) \in [\mathbf{x}_{\min,0}; \mathbf{x}_{\max,0}] \tag{3}$$

$$\mathbf{x}(t_f) \in [\mathbf{x}_{\min,f}; \mathbf{x}_{\max,f}] \tag{4}$$

$$\mathbf{x}(t) \in [\mathbf{x}_{\min}; \mathbf{x}_{\max}] \tag{5}$$

$$\mathbf{u}(t) \in [\mathbf{u}_{\min}; \mathbf{u}_{\max}] \tag{6}$$

On the one hand the cost functional $\mathcal{J}$ is a function of a penalty term Y depending on the initial and final time t_0 and t_f as well as the aircraft's initial and final state $\mathbf{x}(t_o)$ and $\mathbf{x}(t_f)$. On the other hand, $\mathcal{J}$ consists of the temporal integral over a penalty function $\Psi(x(t), u(t), t)$. The magnitudes of Y and Ψ are scaled by the corresponding weighting factors c_Y and c_Ψ as illustrated in Eq. (1). In this study, different cost functionals are used to calculate climate optimized trajectories as well as to re-route trajectories optimally with regard to COC around CRA (see Sections 5.2 and 5.3).

The aircraft state vector is defined as $\mathbf{x} = [\lambda, \varphi, H, v_{\text{TAS}}, m, m_i]^T$ where λ represents the longitude, φ the latitude, H the altitude, v_{TAS} the true airspeed and m the mass of the aircraft. The accumulated masses of the engine emissions are denoted by $m_i (i \in \text{CO}_2, \text{H}_2\text{O}, \text{NO}_x)$. The aircraft's motion is affected by the control vector $\mathbf{u} = [\chi_H, \dot{v}_{\text{TAS}}, \tau]^T$ with χ_H representing the heading angle, $\dot{v}_{\text{TAS}}$ the acceleration and τ the relative thrust which is a function of the actual thrust (Th), the minimum and the maximum thrust $\text{Th}_{\min}$ and $\text{Th}_{\max}$ respectively (see Eq. (7)).

$$\tau = \frac{\text{Th} - \text{Th}_{\min}}{\text{Th}_{\max} - \text{Th}_{\min}} \tag{7}$$

In this study, the dynamic constraints (see Eq. (2)) are described by Eqs. (8)–(13) which together form the aircraft's equations of motion assuming a point-mass model with a variable aircraft mass and three degrees of freedom.

Considering a spherical earth (radius R_E), the derivatives of latitude and longitude with respect to time are obtained using Eqs. (8)–(9) with γ being the flight path angle defined by $\sin\gamma = \frac{\dot{H}}{v_{\text{TAS}}}$.

$$\dot{\lambda} = \frac{v_{\text{TAS}} \cdot \cos\gamma \cdot \sin\chi_H}{(R_E + H) \cdot \cos\varphi} \tag{8}$$

$$\dot{\varphi} = \frac{v_{\text{TAS}} \cdot \cos\gamma \cdot \cos\chi_H}{(R_E + H) \cdot \cos\varphi} \tag{9}$$

The vertical speed of the aircraft is determined by applying the Total Energy Model as shown in Eq. (10). The aerodynamic drag D as well as the maximum and minimum Thrust $\text{Th}_{\min}$ and $\text{Th}_{\max}$ are calculated based on Eurocontrol's BADA 4.0 models (Nuic and Mouillet, 2012).

$$\dot{H} = \frac{[\tau \cdot (\text{Th}_{\max} - \text{Th}_{\min}) + \text{Th}_{\min} - D] \cdot v_{\text{TAS}}}{m \cdot g} - \frac{v_{\text{TAS}} \cdot \dot{v}_{\text{TAS}}}{g} \tag{10}$$

The temporal derivative of the state variable v_{TAS} equals the control input $\dot{v}_{\text{TAS}}$:

$$\dot{v}_{\text{TAS}} = \dot{v}_{\text{TAS}} \tag{11}$$

Aircraft mass change rate ($\dot{m}$) is represented by the negative fuel flow (FF), determined by BADA 4.0 engine performance models.

$$\dot{m} = -\text{FF} \tag{12}$$

Moreover, the emission flows ($\dot{m}_i$) for $i \in \text{CO}_2, \text{H}_2\text{O}, \text{NO}_x$ are obtained by multiplication of the fuel flow (FF) with the corresponding emission index (EI_i) according to Eq. (13). For the emission indices of CO_2 and H_2O a stoichiometric combustion is assumed. In contrast, EI_{NO_x} is calculated based on the Eurocontrol modified Boeing Fuel Flow Method 2 (DuBois and Paynter, 2006; Jelinek et al., 2004).

$$\dot{m}_i = \text{FF} \cdot \text{EI}_i \tag{13}$$

The limitations of control and state variables (see Eqs. (3)–(5)) are given in Table 1.

Table 1
Control and state limitations used in *TOM*.

Variable	Minimum Value	Maximum Value
Limitations of state variables at starting point 0		
λ_0	24.9633°	24.9633°
φ_0	60.3172°	60.3172°
H_0	7610 m	7610 m
$v_{\text{TAS},0}$	241.95 m/s	241.95 m/s
m_0	165,731 kg	233,00 kg
$m_{i,0}$	0 kg	0 kg
Limitations of state variables at final point f		
λ_f	−80.2906°	−80.2906°
φ_f	25.7933°	25.7933°
H_f	7,610 m	7610 m
$v_{\text{TAS},f}$	241.95 m/s	241.95 m/s
m_f	165,731 kg	165,731 kg
$m_{i,f}$	0 kg	10^7 kg
General limitations of state variables		
λ	−120°	30°
φ	10°	85°
H	7610 m	11,840 m
v_{TAS}	241.95 m/s	241.95 m/s
m	165,731 kg	233,00 kg
m_i	0 kg	10^7 kg
General limitations of control variables		
χ_h	0°	360°
$\dot{v}_{\text{TAS}}$	0 m/s^2	0 m/s^2
τ	0	1

The optimal control problem resulting from Eqs. (1)–(6) is then processed by the Matlab toolbox GPOPS-II. GPOPS-II uses a direct approach based on Legendre-Gauss-Radau collocation methods to transform the continuous optimal control problem into a discrete nonlinear programming problem (NLP) (Rao and Patterson, 2014; Patterson and Rao, 2014). Finally, the NLP is solved using the NLP solver IPOPT (Wächter and Biegler, 2006).

3.4. Modeling the economic impact

The economic impact of each flight is described by cash operating costs, including the costs for fuel, crew, maintenance, and navigation and landing fees. The calculation of these costs is based on the direct operating costs (DOC) method developed by Liebeck, (1995). COC are calculated as function of mission time ($t_f - t_0$) and block fuel ($m_0 - m_f$).

$$\text{COC} = f(t_f - t_0, m_0 - m_f) \tag{14}$$

4. Modeling the climate impact

For a preliminary assessment of the methodology climate change functions are calculated for a single time period.

4.1. Calculation of climate change functions

To determine airspaces with high climate sensitivities, reference cruise emissions are first calculated with *TCM*, which serve as input data for *AirClim*. Cruise emissions are simulated for a 6500 m flight of an Airbus 330-200 with varying flight levels (FL250 - FL390) based on BADA 4.0. Travel speeds for the individual flight levels are defined as corresponding fuel-minimal cruise Mach number and calculated with *TOM*, see Table 2.

In a second step, the sensitivity of regional emissions on global mean near surface temperature changes is investigated by releasing the resulting cruise emissions of each flight level into *AirClim*'s emission

Table 2
Fuel-optimal Mach numbers for varying flight levels calculated with *TOM*.

FL	390	350	320	280	250
Ma	0.78	0.76	0.71	0.66	0.62

regions of corresponding height. To estimate the climate mitigation potential of operational, technological and/or regulative concepts, a foreward looking climate metric is needed, which quantifies the future climate change over a defined time horizon caused by CO_2 and non-CO_2 emissions of a particular flight. In order to meet these requirements, the climate response per flight is expressed as average temperature response over 100 years ($ATR_{100,i}$) for each climate agent i:

$$ATR_{100,i} = \frac{1}{100}\int_{t}^{t+100} \Delta T_i(t)\cdot dt \tag{15}$$

The spatial distribution of $ATR_{100,i}(\mathbf{z})$ is normalized by the emissions of corresponding flight level m_i(FL) to generate emission based climate change functions ($eCCF_i$) according to Eqs. (16)–(17):

$$eCCF_i(\mathbf{x}) = \frac{ATR_{100,i}}{m_i(\mathrm{FL})} \quad \text{for } i \in \{CO_2,\ H_2O,\ NO_x\} \tag{16}$$

$$eCCF_{CiC}(\mathbf{x}) = \frac{ATR_{100,i}}{d(\mathrm{FL})} \quad \text{for } i \in \{\mathrm{CiC}\} \tag{17}$$

Total climate change functions of a specific month, which form the decisive basis for the definition of climate restricted areas, are obtained by superposition of eCCF i:

$$CCF_{tot}(\mathbf{x}) = \sum_i \underbrace{eCCF_i(\mathbf{x})\cdot m_i(\mathbf{x})}_{CCF_i(\mathbf{X})} + \underbrace{eCCF_{CiC}(\mathbf{x})\cdot d(\mathrm{FL})}_{CCF_{CiC}(\mathbf{X})} \tag{18}$$

eCCF are calculated between +15° and +80° northern latitude and between −130° and +30° eastern longitude for an altitude range of $H_{min} = 7,610$ m and $H_{max} = 11,840$ m. They are plotted in Fig. 1 as function of altitude and latitude, and in Fig. 2 as function of longitude and latitude of the emission (Miller projection). The climate sensitivity of all considered climate agents, except CH_4, is increasing with rising altitudes. Since the formation of contrails extracts water vapor out of the air, water vapor saturation of a region is decreasing with increasing traffic volume. This effect leads to a saturation of the contrail coverage in regions with high air traffic flows. Hence, the climate impact of CiC of a single mission tends towards zero over middle Europe, the USA, and at the North Atlantic Tracks (NATs); compare Fig. 2b. Maximum and minimum values of $eCCF_{tot}$ are reached over the Caribbean Sea. Peak values occur at the maximum permitted altitude $H_{max} = 11,840$ m; minimum values in an altitude $H = 8,596$ m.

It has to be mentioned explicitly, that the calculation of climate change functions is associated with uncertainties, since research of the climate impact of individual components is still in progress. However, the relation of the environmental impact of the climate agents and spatial variability is more important for the trajectory optimization than absolute values (Dahlmann et al., 2016).

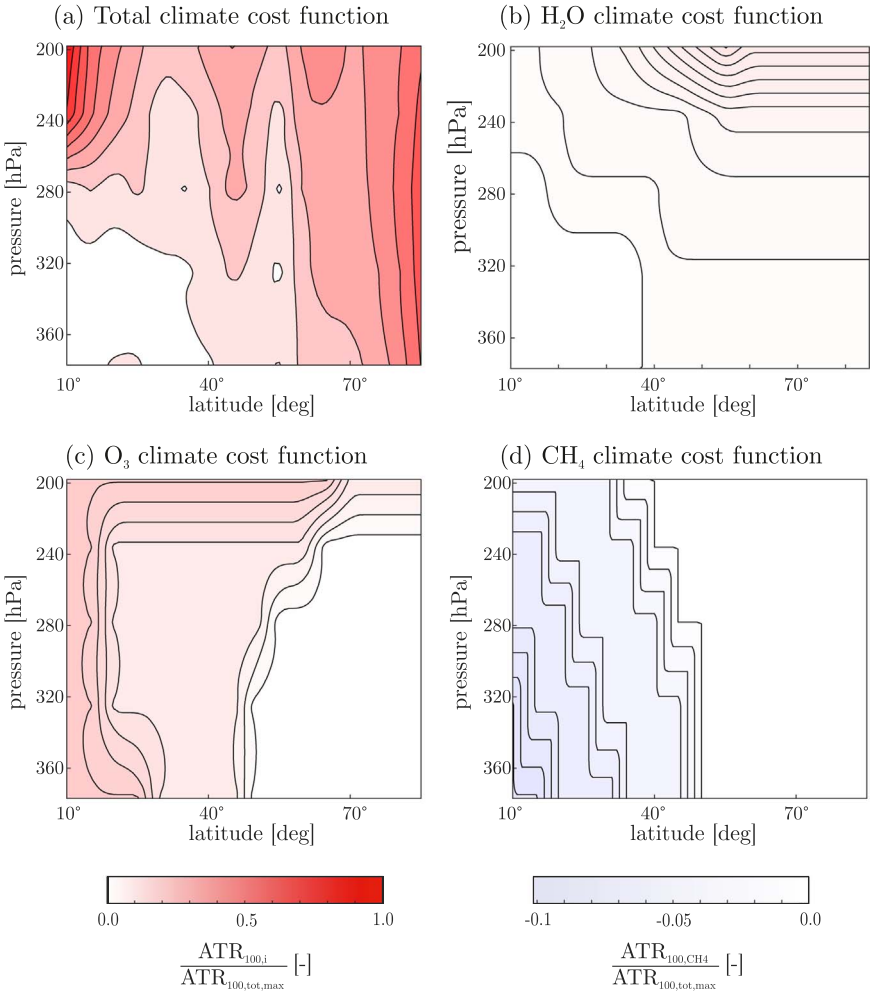

Fig. 1. Absolute climate change functions (CCF) at the Greenwich meridian as function of altitude and latitude derived with *AirClim*. Figures show CCF of (a) all considered climate agents, (b) water vapor, (c) ozone, and (d) methane.

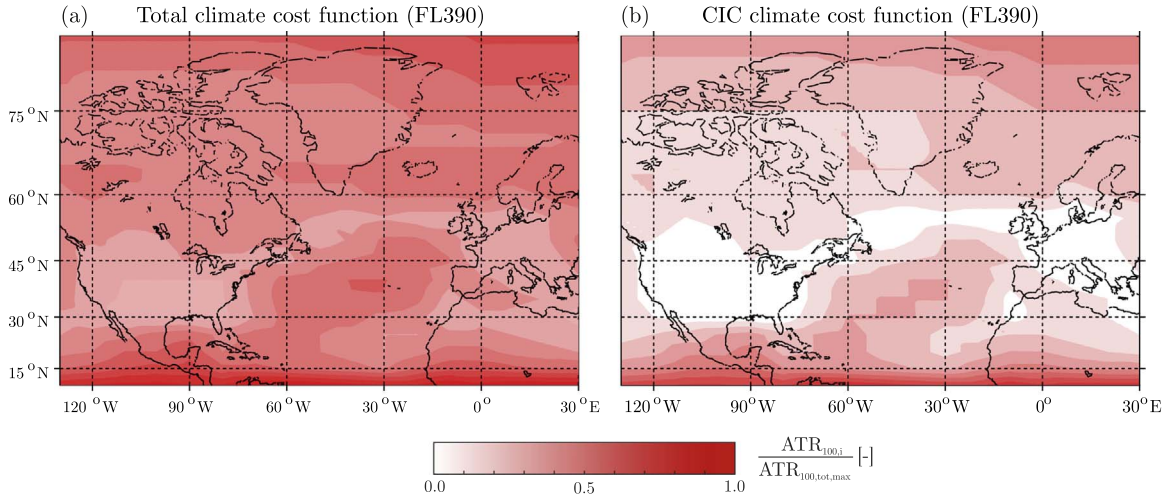

Fig. 2. Absolute climate change functions (CCF) at 39,000 ft as function of latitude and longitude derived with *AirClim*. Figure (a) depicts the CCF of all considered climate agents, and (b) the CCF of contrail induced cloudiness (CiC).

4.2. Definition of climate restricted airspaces

Based on the scale of total climate costs (see Figs. 1 and 2.a), climate restricted areas are defined by the selection of a threshold value. Airspaces are closed if CCF_{tot} exceeds the chosen threshold value (c_{thr}); others are cleared for air traffic. Fig. 3 shows the resulting climate restricted airspace of varying flight altitudes over the North-Atlantic and adjoining countries for a threshold value of $c_{thr} = 0.390$.

In accordance with increasing scale of climate sensitivity of aircraft emissions with altitude, more and more airspaces are restricted in higher flight levels; compare Fig. 1a, Figs. 2 and 3.

5. Trajectory calculation

In a first single-mission assessment of climate restricted airspaces, we focus on the trans-Atlantic route from Helsinki, Finland (EFHK) to Miami, USA (KMIA).[1] Flight simulations are performed on this route to calculate changes in cruise emissions and time for varying threshold values. The resulting data is used to estimate the corresponding changes in cash operating costs and average temperature response.

All trajectories are simulated with a BADA 4.0 Airbus A330-200 aircraft performance model, assuming International Standard Atmosphere (ISA) conditions (no wind). Each trajectory is simulated with a load factor of 85%, a reserve fuel mass equivalent to 5% of the fuel required for the reference trajectory (2646 kg). Infrastructural constraints and operational ATC restrictions are neglected. Further boundary conditions for trajectory calculations are presented in Table 1.

5.1. Calculation of reference trajectory

For comparison purposes, a great circle trajectory with constant Mach number (Ma = 0.82) and constant flight altitude (FL380) is simulated with *TCM*. COC and ATR of the reference case serve as a benchmark for the following cost-benefit analysis.

5.2. Calculation of optimized trajectories with respect to climate and economy

Since the objective functions 'minimum COC' and 'minimum ATR' can be contradictory, no single solution must exist that simultaneously minimizes both of them. Hence, a multi-objective optimization is necessary to derive optimized trajectories with respect to climate and economy. To perform such a multi-objective optimization, we integrate monetary (COC) and emission based climate change functions ($eCCF_i$) into *TOM*'s cost functional $\mathcal{J}$, see Eq. (1). *TOM* generates Pareto optimal solutions by minimizing $\mathcal{J}_{CCF}$ with varying monetary (c_Y) and climate weighting factors (c_Ψ), as defined in Eqs. (19) and (20):

$$\mathcal{J}_{CCF} = c_Y \cdot COC(t_f - t_0,\, m_0 - m_f) \cdot COC_{ref}^{-1} + c_\Psi \cdot \underbrace{\left(\sum_i \int_{t_0}^{t_f} eCCF_i(\mathbf{x}) \cdot \dot{m}_i \cdot dt + \int_{t_0}^{t_f} eCCF_{CiC}(\mathbf{x}) \cdot v_{TAS}(t) \cdot dt \right)}_{ATR_{100,tot}} \times (ATR_{100,tot,ref})^{-1} \quad (19)$$

$$c_Y + c_\Psi = 1 \quad \text{with } c_Y,\, c_\Psi \in [0,\, 1] \quad (20)$$

The resulting trajectory is optimal with regard to COC, if $c_Y = 1$; it is optimal with regard to climate, if $c_\Psi = 1$. All other perturbations of c_Y and c_Ψ are Pareto optimal, for which ATR cannot be improved in value without degrading COC. Fig. 4 illustrates various lateral flight trajectories for the selected city pair connection from Helsinki to Miami; plotted as Miller projection. The optimal trajectory with respect to COC ($c_\Psi = 0$) matches the shortest connection (great circle as no wind considered). With an increasing climate weighting factor c_Ψ, the trajectories are shifted to regions with lower climate sensitivities while flight distance, flight time and fuel burn are increasing; see Table 3. In our case, the climate-optimal trajectory is located at lower latitude to avoid contrail formation.

The vertical flight profile (Fig. 5a) of the optimal trajectory with regard to COC is a continuous climb. The kink in the middle of the route is caused by the change of the temperature gradient in the tropopause. Maximum permitted flight altitude ($H_{Max} = 11,840$ m) is reached at $t/t_f \approx 0.75$ of the cruise flight.

As total climate costs increase with rising altitudes, flights with increasing c_Ψ are performed in lower flight altitudes (see Fig. 5b–d). These results are in agreement with the climate mitigation studies published by Koch et al. (2012). In contrary to Koch et al, we do not adapt the flight speed to the flight altitude in this study. All flights are performed with a constant true airspeed $v_{TAS} = 241.95$ m/s (Ma0.82@11, 000 m). Hence, the total mitigation potential might even be larger than calculated.

[1] The EFHK-KMIA route is selected for trajectory optimization due to high vertical and lateral climate change gradients in-between.

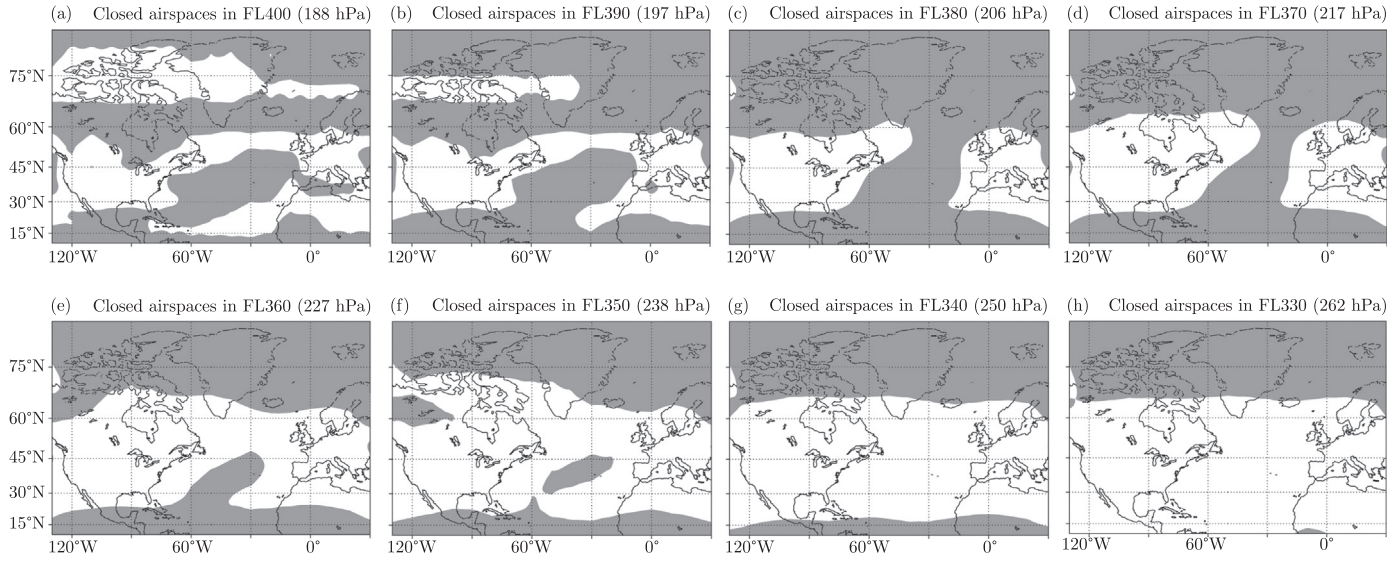

Fig. 3. Climate restricted airspaces (CRA, gray-colored) between 15° and 80° northern latitude and between −130° and 30° eastern longitude. Airspaces are closed if the climate sensitivity exceeds the chosen threshold value. Figures (a) to (h) depict restricted airspaces of different flight altitudes (FL250 to FL390) for a chosen threshold value of $c_{thr} = 0.390$..

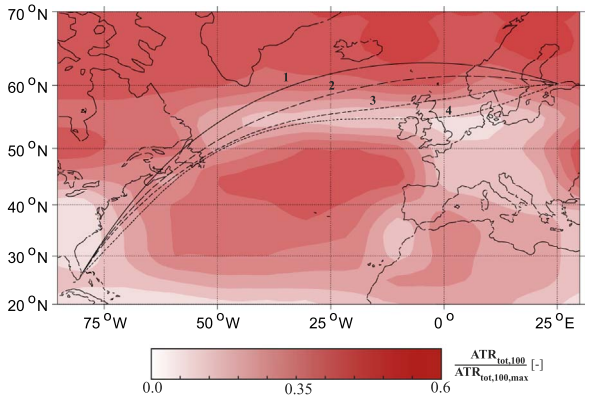

Fig. 4. Latitude - longitude plots of climate optimized trajectories (COT) on the trans-Atlantic route from Helsinki, Finland (EFHK) to Miami, USA (KMIA) with varying climate weighting factors (c_Ψ). CCF are pictured for a mean flight altitude of these four trajectories of 9635 m. Black lines represent optimal trajectories for (1) $c_\Psi = 0.0$ (optimal with respect to COC), (2) $c_\Psi = 0.042$, (3) $c_\Psi = 0.122$, and (4) $c_\Psi = 1.0$ (optimal with respect to ATR).

Table 3
Cash operating costs (COC) and average temperature response (ATR) for climate optimized trajectories (COT) on the trans-Atlantic route from Helsinki, Finland (EFHK) to Miami, USA (KMIA). The trajectory is optimal with regard to COC, if $c_\Psi = 0$ or $c_{thr} = 0$; it is optimal with regard to climate, if $c_\Psi = 1$.

Climate optimized trajectories					
COC [−]	$ATR_{100,tot}$ [−]	c_Ψ [−]	**mean Alt.** [m]	**Fuel** [−]	**Time** [−]
0.995	0.975	0.000	11,054	0.988	1.002
1.000	0.880	0.019	10,593	0.997	1.003
1.014	0.762	0.042	10,030	1.025	1.006
1.020	0.735	0.061	9,539	1.034	1.009
1.032	0.700	0.073	9,539	1.058	1.011
1.040	0.673	0.087	9,424	1.071	1.016
1.055	0.632	0.122	9,203	1.096	1.023
1.060	0.623	0.138	9,145	1.104	1.026
1.080	0.595	0.280	8,865	1.138	1.036
1.100	0.582	0.523	8,464	1.174	1.043
1.111	0.578	1.000	8,319	1.193	1.048

5.3. Re-Routing of trajectories around climate restricted airspaces (CRA)

Analogous to the calculation of optimized trajectories, COC and CRA are integrated into *TOM* to minimize the CRA cost functional ($\mathcal{J}_{CRA}$), which is calculated according to Eq. (21):

$$\mathcal{J}_{CRA} = c_\Upsilon \cdot COC(t_f - t_0,\, m_0 - m_f) COC_{ref}^{-1} + c_\Psi \cdot \int_{t_0}^{t_f} CRA(\mathbf{x}) \cdot dt \tag{21}$$

Climate penalties are implemented as one in those areas in which CCF ($\mathbf{x}$) exceed the threshold value c_{thr}; otherwise climate penalties are zero, see Eq. (22):

$$CRA(\mathbf{x}) = \begin{cases} 1\ s^{-1}, & \text{if } CCF_{100,tot}(\mathbf{x}) \geq c_{thr} \\ 0, & \text{if } CCF_{100,tot}(\mathbf{x}) < c_{thr} \end{cases} \tag{22}$$

In order to ensure that no trajectory passes restricted areas, a high climate weighting factor ($c_\Psi = 0.99$) is selected.

Since the share of climate penalties of $\mathcal{J}_{CRA}$ tends towards zero with this methodology, $\mathcal{J}_{CRA}$ is exclusively dependent on monetary costs functions. Thus, *TOM* creates optimal trajectories with regard to COC under the constraint of avoiding CRA for varying c_{thr}.

For $c_{thr} = 1$ the total airspace is cleared for air traffic. Thus, the optimal trajectory with regard to COC is identical to that of Section 5. With decreasing c_{thr}, the restriction is getting stricter, and more and more airspaces are closed. To specify the restricted volume fraction of the total airspace we introduce the parameter ϕ_{CRA}, which is defined as the volume of CRA (V_{CRA}) divided by the volume of the total airspace (V_{tot}):

$$\phi_{CRA} = \frac{V_{CRA}}{V_{tot}}, \quad \in [0,\, 1] \tag{23}$$

Fig. 6 shows the lateral profile for CRA avoiding trajectories for varying threshold values. CRA of each threshold value is illustrated in a different shade of gray in an altitude of 10,289 m. Areas, which are colored in dark-gray, will be closed first. Corresponding COC, ATR and ϕ_{CRA} values for different threshold values are shown in Table 4.

Similar to climate optimized trajectories, the re-routed ones are shifted to lower altitudes with decreasing c_{thr}, see Fig. 7. As cleared airspace is decreasing with decreasing c_{thr}, the entire traffic demand has to be handled within the remaining airspace, which strongly influences flight frequencies as well as controller workload. This might lead to a capacity crunch.

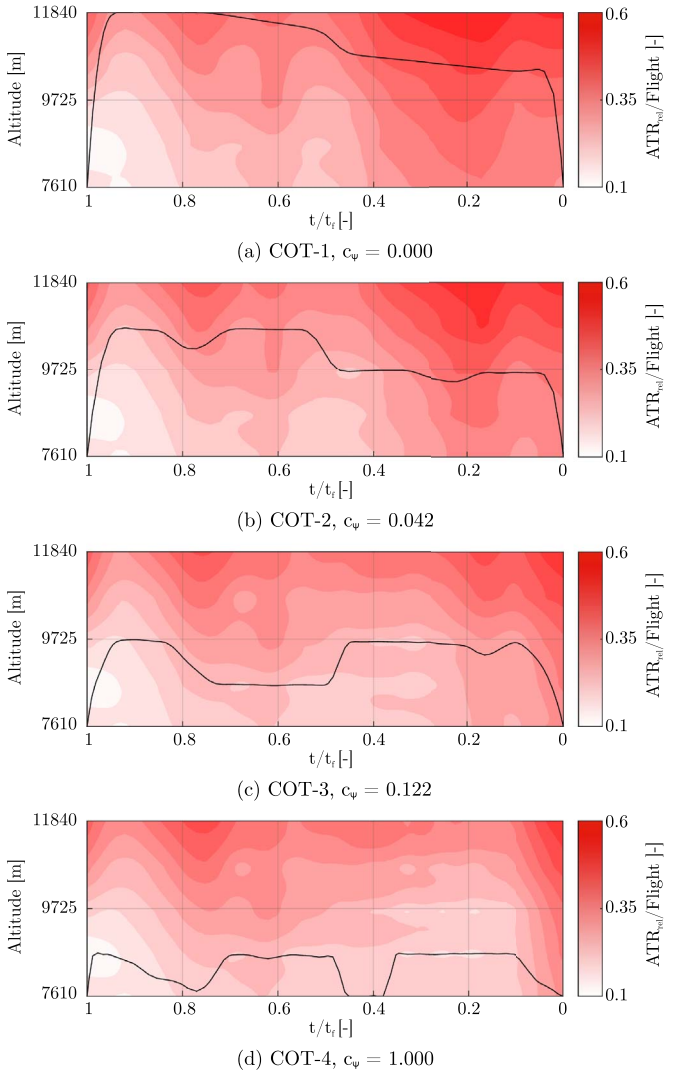

Fig. 5. Altitude - flight time plots of climate optimized trajectories (COT) on the trans-Atlantic route from Helsinki, Finland (EFHK) to Miami, USA (KMIA) with varying climate weighting factors (c_{Ψ}). $CCF_{100,tot}$ are pictured along the cross section of the lateral path. Figures represent optimal trajectories for (a) $c_{\Psi} = 0.0$ (optimal with regard to COC), (b) $c_{\Psi} = 0.042$, (c) $c_{\Psi} = 0.122$, and (d) $c_{\Psi} = 1.0$ (optimal with respect to ATR).

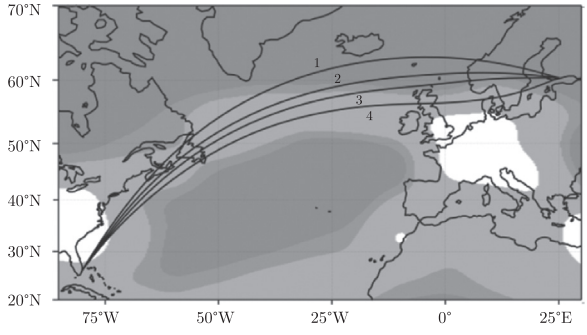

Fig. 6. Latitude - longitude plots of CRA avoiding trajectories on the trans-Atlantic route from Helsinki, Finland (EFHK) to Miami, USA (KMIA) with varying climate weighting factors (c_{Ψ}). CRA of varying threshold values (c_{thr}) are pictured in different shades of gray for an mean altitude of 10,289 m: 1: $c_{thr} = 1.0$ (total airspace cleared for air traffic); 2: $c_{thr} = 0.390$; 3: $c_{thr} = 0.354$; 4: $c_{thr} = 0.248$. Black lines represent trajectories for corresponding threshold values.

If the threshold value tends towards zero, nearly the complete airspace is closed and no flights can be operated any more. For the selected route, the maximal reduction of the climate impact is reached for a threshold value of 0.248 ($\phi_{CRA} = 0.668$), as the airspace over Helsinki will be completely closed for lower values (compare Fig. 7d).

6. Effectiveness of climate restricted routing

In the previous sections trajectory simulations are performed to estimate cash operating costs and average temperature responses for varying trajectories on the trans-Atlantic route from Helsinki to Miami. For the simulations of trajectories infrastructural constraints in flight planning have to be taken into account, which may impact the actual mitigation potential. Thus, the resulting gross cost-benefit potential of both strategies may be less than calculated here. Since all calculations are based on climatological mean data without wind information, wind effects are not considered.[2] These results are used to assess the cost-benefit potential (COC vs. ATR) of both strategies. Fig. 8 shows the increment of COC, against ATR reduction. Each black dot represents a Pareto element of climate optimized trajectories; each red dot represents a Pareto element of CRA avoiding trajectories.

Considering the relevance of economic efficiency for the airlines, the most desirable trajectory modifications mitigate the net climate impact by the most while incrementing the operating costs by the least. In our cases, we can mitigate the climate impact without any increase of cash operating costs either by 12.0% by minimizing time and emissions in regions with high climate sensitivities, or by 8.7% by closing 28.8% of the total airspace. If a cost penalty is accepted, global warming can be reduced even more; such as by 26.5% for climate-optimized or by 21.9% for CRA avoiding trajectories ($\phi_{CRA} = 0.479$), if a cash operating cost increment of 2.0% is selected. Since the environmental impact of aviation is highly dependent on the locus of non-CO_2 emissions, its effect is reducible although fuel burn and corresponding aircraft emissions are increasing. Vertically all trajectories are shifted to lower flight altitudes.

The comparison of vertical and lateral flight profiles of both strategies also shows that it is often more environmental friendly to pass highly climate sensitive regions for a short time as to avoid them totally. Longer detours of CRA avoiding trajectories induce, i.e. for an ATR improvement of 30.0% an increase of 1.9% for fuel consumption and 1.7% for flight time compared with climate optimized trajectories, resulting in 1.6% higher cash operating cost (total COC_{CRA} increment is 4.8%, compare Tables 3, 4). For that reason, climate optimized trajectories always achieve higher climate mitigation potentials as CRA avoided ones at same cost penalties.

It is important to note, that the goal of our research is to shape the predicted growth of air traffic in a climate neutral way, not to reduce or prevent it. Obviously such strict restrictions of the airspace would lead to a capacity crunch of the air transportation system and are, hence, neither implementable nor expedient. It is for this reason that we need to assess the climate mitigation potential of monthly CRA with small thresholds in a global aircraft network. Furthermore, it is also conceivable to introduce different ATM charges for flights through climate sensitive regions; instead of closing them totally (soft constraints for CRA).

Nevertheless, these first results indicate, that CRA may be a promising interim mitigation strategy, as they are easily implementable and its gross cost-benefit potentials are close by for small cost penalties. If re-routing of flights around CRA is limited to the most ecologically harmful trajectories, it may pave the way for a prompt reduction of global warming without capacity crunch of the air transportation system.

[2] The influence of wind on optimized flight trajectories with regard to monetary and climate cost is addressed i.a. by Lührs et al. (2016).

Table 4
Cash operating costs (COC) and average temperature response (ATR) for CRA avoiding trajectories on the trans-Atlantic route from Helsinki, Finland (EFHK) to Miami, USA (KMIA) for varying threshold values (c_{thr}).

CRA avoiding trajectories						
COC [−]	$ATR_{100,tot}$ [−]	c_{thr} [−]	ϕ_{CRA} [−]	**mean Alt.** [*m*]	**Fuel** [−]	**Time** [−]
0.995	0.975	1.000	0.000	11,054	0.988	1.002
1.000	0.913	0.418	0.288	10,761	0.997	1.003
1.005	0.880	0.390	0.362	10,660	1.004	1.006
1.015	0.805	0.354	0.440	10,353	1.020	1.012
1.020	0.781	0.336	0.479	10,245	1.028	1.016
1.040	0.725	0.297	0.563	9730	1.063	1.024
1.048	0.700	0.281	0.597	9591	1.077	1.028
1.060	0.654	0.263	0.635	9331	1.098	1.033
1.071	0.640	0.248	0.668	9125	1.118	1.036

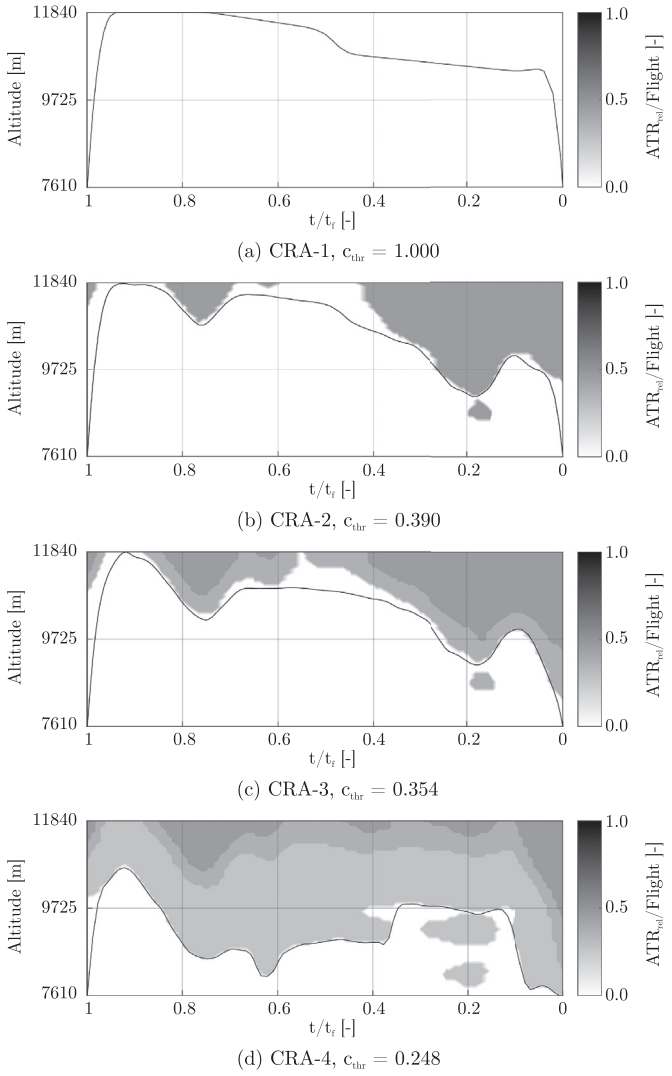

Fig. 7. Altitude - longitude plots of CRA avoiding trajectories on the trans-Atlantic route from Helsinki, Finland (EFHK) to Miami, USA (KMIA) with varying climate weighting factors (c_{Ψ}). CRA are pictured along the cross section of the lateral path. Figures represent re-routed trajectories for (a) c_{thr} = 1.0 (total airspace cleared for air traffic), (b) c_{thr} = 0.390, (c) c_{thr} = 0.354, and (d) c_{thr} = 0.248.

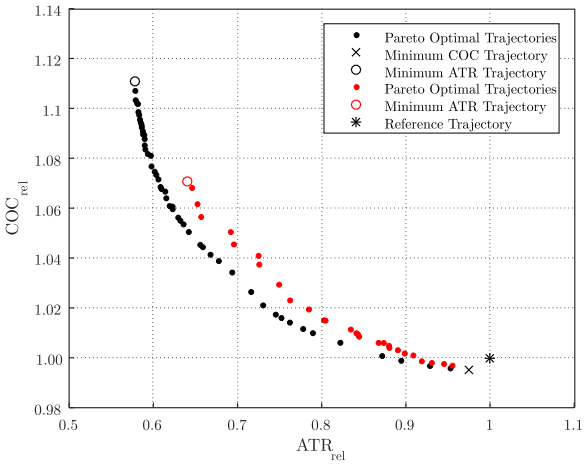

Fig. 8. Pareto fronts of climate reduction potential (ATR) and cash operating costs (COC) for the trans-Atlantic route from Helsinki, Finland (EFHK) to Miami, USA (KMIA). Black dots represent the Pareto front for climate optimized trajectories; red dots represent the Pareto front for re-routed trajectories around CRA. Reference trajectory (great circle flight in a constant flight altitude) is depicted as star symbol.

7. Conclusion and outlook

The objective of this research was to develop a methodology of a climate mitigation strategy, which can be easily implemented in the next few years and bridges the time period until the most promising mitigation strategies are feasible. To realise this, we introduce climate restricted airspaces, in analogy to military exclusion zones, and re-route affected flights around them.

For an ecological and economic assessment of this interim mitigation strategy a simulation framework was developed. First, 3-D climate change functions (CCF) have been calculated, which characterize the environmental impact caused by an aircraft emission at a certain location. They are used both, as penalty function for the climate optimization of trajectories, and as decision variable for the definition of climate restricted areas. Based on the scale of total CCF, a threshold value is selected, which defines the boundary condition between restricted and cleared airspace. Regions with climate costs greater than the threshold value are closed; others are cleared for air traffic. To detour flights optimally with regard to COC around the resulting CRA, optimal control techniques are applied. For each optimized flight trajectory the corresponding average temperature response and cash operating costs are expressed relatively to a reference great circle trajectory with constant Mach number.

A preliminary cost-benefit analysis of this strategy on the route from Helsinki (EFHK) to Miami (KMIA) indicates that there exist large potentials to mitigate the global warming of aviation without any increase of cash operating costs, either by 12.0% by climate optimized, or by 8.7% by CRA avoided trajectories, if 28.8% of the total airspace is closed. However, such strict restrictions of the airspace would lead to a capacity crunch of the air transportation system. To shape the predicted growth of air traffic in a climate neutral way without reducing or preventing it, re-routing of flights around CRA should be limited to the most ecologically harmful trajectories.

In future publications we are planning to extend our analysis to network level and to integrate airspace capacity constraints. Wind effects will be integrated by applying the methodology for consideration of long term wind effects according to Swaid et al. (2016). Also seasonal dependencies of aircraft emissions on climate shall be taken into account in the next studies. For that purpose, pre-calculated atmospheric data of *AirClim*, which is derived from E39/C, shall be evaluated separately for every month to calculate monthly climate change functions. In this way, we limit the re-routing activities to the most ecologically harmful trajectories in the seasons with the highest climate impact; contrary to many other climate mitigation strategies, which propose permanent trajectory changes. Furthermore, it is also conceivable to introduce different ATM charges for flights through climate sensitive regions; instead of closing them totally.

Acknowledgments

We thank Jesper van Manen and Alexander Lau for their support of this paper, and Eurocontrol for providing BADA 4.0 data.

References

Airbus, Global market forecast: Future journeys 2013–2032 (2013).

Borken-Kleefeld, J., Steller, H., Ceuster, G.d., Vanhove, F., Eide, M., Endresen, O., Behrens, H., Lee, D., Owen, B., Meretei, T., Rypdal, K., Skeie, R., van Aardenne, J., Erhardt, G., Sausen, R., 2010. Quantify transport emission scenarios up to 2100. Environ. Sci. Technol. 44. http://dx.doi.org/10.1021/es9039693, (55700–5706).

Dahlmann, K., Grewe, V., Frömming, C., Burkhardt, U., 2016. Can we reliably assess climate mitigation options for air traffic scenarios despite large uncertainties in atmospheric processes? Transp. Res. D.-TR E 46, 40–55. http://dx.doi.org/10.1016/j.trd.2016.03.006.

DuBois, D., Paynter, G., 2006. Fuel flow method 2 for estimating aircraft emissions.

Grewe, V., Stenke, A., 2008. Airclim: an efficient tool for climate evaluation of aircraft technologies. Atmos. Chem. Phys. 8, 4621–4639. http://dx.doi.org/10.5194/acp-8-4621-2008.

Grewe, V., Frömming, C., Matthes, S., 2014. Aircraft routing with minimal climate impact: the REACT4C cost function modelling approach. Geosci. Model Dev. 7, 175–201. http://dx.doi.org/10.5194/gmd-7-175-2014.

Henderson, S.C., Wickrama, U.K., Baughcum, S.L., Begin, J.J., Franco, F., Greene, D.L., Lee, D.S., McLaren, M.L., Mortlock, A.K., Newton, P.J., Schmitt, A., Sutkus, D.J., Vedantham, A., Wuebbles, D.J., 1999. Aircraft emissions: current inventories and future scenarios. In: Penner, J.E., Lister, D.H., Griggs, D.J., Dokken, D.J., McFarland, M. (Eds.), Aviation and the Global Atmosphere, Intergovernmental Panel on Climate Change. Cambridge University Press, UK.

Houghton, J., Ding, Y., Griggs, D., Noguer, M., van der Linden, P., Dai, X., Maskell, K., Johnson, C., 2001. Climate change 2001: the Scientific Basis. Contribution of working group I to the third assessment report of the intergovernmental panel on climate change, Cambridge University Press, Cambridge, New York, Madrid, Cape Town, Singapore, Sao Paolo, Delhi.

Jelinek, F., Carlier, S., Smith, J., 2004. Advanced emission model (AEM3) v1.5 validation report.

Koch, A., Lührs, B., Linke, F., Gollnick, V., Dahlmann, K., Grewe, V., Schumann, U., Otten, T., Kunde, M., 2012. Climate-compatible air transport system: Climate impact mitigation potential for actual and future aircraft, TAC-3 Proceedings.

Lührs, B., Linke, F., Gollnick, V., 2014. Erweiterung eines Trajektorienrechners zur Nutzung meteorologischer Daten für die Optimierung von Flugzeugtrajektorien. Ger. Aerosp. Congr. (DLRK) 63.

Lührs, B., Niklass, M., Frömming, C., Grewe, V., Gollnick, V., 2016. Cost-benefit assessment of 2d and 3d climate and weather optimized trajectories, AIAA Aviation Technology, Integration, and Operations Conference (ATIO), 16, Washington, D.C.

Lee, D., Pitari, G., Grewe, V., Gierens, K., Penner, J., Petzold, A., Prather, M., Schumann, U., Bais, A., Berntsen, T., Iachetti, D., Lim, L., Sausen, R., 2010. Transport impacts on atmosphere and climate: Aviation. Atmos Environ. 44, 4678–4734. http://dx.doi.org/10.1016/j.atmosenv.2009.06.005.

Liebeck, R., 1995. Advanced subsonic airplane design and economic studies. NASA CR-195443.

Linke, F., 2016. Ökologische Analyse operationeller Lufttransportkonzepte, (Ph.D. thesis), Hamburg University of Technology (TUHH), Hamburg.

Mulkerin, T., 2003. Free flight is in the future: Large-scale controller pilot data link: Communications emulation testbed. IEEE Aerosp. Electron. Syst. Mag. 18, 23–27. http://dx.doi.org/10.1109/MAES.2003.1232156.

Nuic, A., Mouillet, V., 2012. User manual for the base of aircraft data (BADA) family 4, ECC Tech./Scien., Report No. 12/11/22-58.

Patterson, M.A., Rao, A.V., 2014. GPOPS-ii A matlab software for solving multiple-phase optimal control problems using hp-adaptive gaussian quadrature collocation methods and sparse nonlinear programming. ACM Trans. Math. Softw. 49, 1:1–1:37.

Rädel, G., Shine, K., 2010. Validating ECMWF forecasts for the occurrence of ice supersaturation using visual observations of persistent contrails and radiosonde measurements over England. Q. J. R. Meteorol. Soc. 136, 1723–1732. http://dx.doi.org/10.1002/qj.670.

Rao, A.V., Patterson, M.A., 2014. GPOPS-ii - a general-purpose MATLAB software for solving multiple-phase optimal control problems.

SESAR, The roadmap for sustainable air traffic management: European ATM master plan (2012).

Solomon, S., Qin, D., Manning, M., Chen, Z., Marquis, M., Averyt, K., Tignor, M., Miller, H. (Eds.), 2007. Climate change 2007: The Physical Science Basis. Contribution of Working Group I to the Fourth Assessment Report of the Intergovernmental Panel on Climate Change (IPCC), Cambridge University Press, Cambridge, New York, Madrid, Cape Town, Singapore, Sao Paolo, Delhi.

Swaid, M., Lührs, B., Linke F., Gollnick, V., Cai, K.Q., 2016. Wind-optimal ATS route redesign: A methodology and its application to route A461 in china, AIAA Aviation Technology, Integration, and Operations Conference (ATIO), 16, Washington, D.C.

Wächter, A., Biegler, L.T., 2006. On the implementation of an interior-point filter line-search algorithm for large-scale nonlinear programming. Math. Program. 106.